Mechanical Systems and Signal Processing 81 (2016) 360–374

Contents lists available at ScienceDirect

Mechanical Systems and Signal Processing

journal homepage: www.elsevier.com/locate/ymssp

Design of MEMS piezoelectric harvesters with electrostatically adjustable resonance frequency

H. Madinei, H. Haddad Khodaparast*, S. Adhikari, M.I. Friswell

College of Engineering, Swansea University, Bay Campus, Fabian Way, Crymlyn Burrows, Swansea, SA1 8EN, United Kingdom

ARTICLE INFO

Article history:
Received 13 October 2015
Received in revised form
4 March 2016
Accepted 31 March 2016
Available online 18 April 2016

Keywords:
MEMS devices
Piezoelectric
Energy harvesting
Harmonic balance

ABSTRACT

In this paper the analytical analysis of an adaptively tuned piezoelectric vibration based energy harvester is presented. A bimorph piezoelectric energy harvester is suspended between two electrodes, subjected to a same DC voltage. The resonance frequency of the system is controllable by the applied DC voltage, and the harvested power is maximized by controlling the natural frequency of the system to cope with vibration sources which have varying excitation frequencies. The nonlinear governing differential equation of motion is derived based on Euler Bernoulli theory, and due to the softening nonlinearity of the electrostatic force, the harvester is capable of working over a broad frequency range. The steady state harmonic solution is obtained using the harmonic balance method and results are verified numerically. The results show that the harvester can be tuned to give a resonance response over a wide range of frequencies, and shows the great potential of this hybrid system.

1. Introduction

Energy harvesting technologies that rely on the conversion of ambient vibration into a usable form of energy have become the subject of significant research topic in recent years [1–9]. The most common types of transduction methods are piezoelectric [10], electromagnetic [11] and electrostatic [12]. Among these three methods, piezoelectric convertors have been recognized to offer more benefits. They have presented a potential solution to power systems which have a short battery life and high maintenance costs. The battery replacement is more of a problem for Micro Electro Mechanical Systems (MEMS). For some application it is not often practical to replace the dead battery because they are not easily accessible. Therefore, the concept of low-power MEMS devices that are able to scavenge, or harvest, energy from their operating environment have gained growing attention over recent years [13–15].

A MEMS-scale energy converter employing a piezoelectric thin film was first reported in 2005 by Jeon et al. [16]. They studied a 170 μm $\times$ 260 μm PZT beam power generator that can harvest 1 μW power output across a 5.2 MΩ resistive load from a 10.8 g vibration at its resonance frequency of 13.9 kHz. Subsequently, a second generation of Piezoelectric Micro Power Generator (PMPG) was proposed by the same group [17]. They considered the effect of proof mass, beam shape and damping on the performance of the system and showed that the maximum harvested power occurs when the resonance frequency of the energy harvester matches the dominant excitation frequency. Renaud et al. [18] reported the fabrication, modeling, and characterization of a MEMS piezoelectric cantilever power generator with an integrated proof mass that can

* Corresponding author.
E-mail address: h.haddadkhodaparast@swansea.ac.uk (H.H. Khodaparast).

http://dx.doi.org/10.1016/j.ymssp.2016.03.023
0888-3270/

generate an average power of 40 μW at 1.8 kHz. Shen et al. [19] designed a MEMS piezoelectric energy harvesting device for low vibration frequency and high vibration amplitude environment. They showed that with beam dimensions of 4.8 mm × 0.4 mm × 0.036 mm, 2.15 μW power can be harvested at 461.15 Hz.

Most of energy harvesters are designed to work at resonance frequency in order to obtain maximum output power, and they are usually manufactured to have natural frequencies that match the frequencies of excitation. However in some cases, there is a mismatch between the natural and excitation frequencies due to manufacturing errors or changes in the working condition. To overcome this problem, harvesters with adjustable natural frequencies [20] and multiple oscillators [21] have been proposed to improve the performance of the harvesters. Furthermore, the use of damping to allow better extraction over a broad frequency band [22] and the use of nonlinear behavior [23] and magnetic buckling [24] have been exploited to harvest energy efficiently over a wider frequency range.

There are different concepts through which the resonance frequency of the harvester can be tuned. Marzencki et al. [25] employed mechanical nonlinear strain stiffening to tune the resonance frequency of a MEMS vibration energy harvester. Zhu et al. [26] used permanent magnets to adjust the natural frequency of an electromagnetic micro-generator. They showed that by applying different axial tensile forces to the micro-generator, the natural frequency of the system can be tuned. Challa et al. [27] investigated a vibration energy harvesting device with autonomously tunable resonance frequency. They used a piezoelectric cantilever beam array with magnets attached to the free ends of cantilever beams to tune resonance frequency of the system by magnetic force. More recently, Miller et al. [28] proposed a passive self-tuning beam resonator with sliding proof mass along the beam. This model enables the energy harvesting system to adjust the natural frequency of the system and thereby increase the energy harvested over time.

This paper presents a comprehensive study and a framework for the design of a MEMS piezoelectric harvester which employs an electrostatic device to adjust its resonance frequency. The paper builds upon previous work published by the authors (Madinei et al. [29]), where the behavior of the harvester was numerically studied. In this work, we develop an analytical solution using Harmonic Balance in order to efficiently solve the governing equations of the proposed harvester. To this end, the nonlinear term of the electrostatic force is expanded using a Taylor series and the terms higher than the ninth order are neglected (based on a convergence study). Using a Galerkin based reduced order model, a single-degree-of-freedom (SDOF) system with nonlinearity up to ninth order is achieved. The steady state response of the harvester is obtained based on the harmonic balance method which is more efficient than direct time integration. The results are verified numerically and the effect of different parameters on the performance of the harvester is investigated in the design of the harvester. Due to the softening nonlinearity of the electrostatic force, the operational frequency range of the harvester can be increased in comparison with the linear tunable models. Finally a framework for the design of such harvesters is proposed and illustrated using a numerical example.

2. Model description and mathematical modeling

Fig. 1 shows the model used in this paper. The model is an isotropic microbeam of length L, width a, thickness h, density ρ and Young's modulus E, sandwiched with piezoceramic layers having thickness h_0, Young's modulus E_0 and density ρ_0 throughout the microbeam length and located between two electrodes (electrode 1 and electrode 2). As illustrated in Fig. 1, the piezoceramic layers are connected to the resistance (R) and the coordinate system is attached to the middle of the left end of the microbeam where x and z refer to the horizontal and vertical coordinates respectively. The tip mass is used to control the dynamics of the micro-cantilever. When the tip mass is much larger than the mass of the cantilever beam, a simple SDOF model can be used to model the harvester. The governing equation of transverse motion can be written as [30,31]

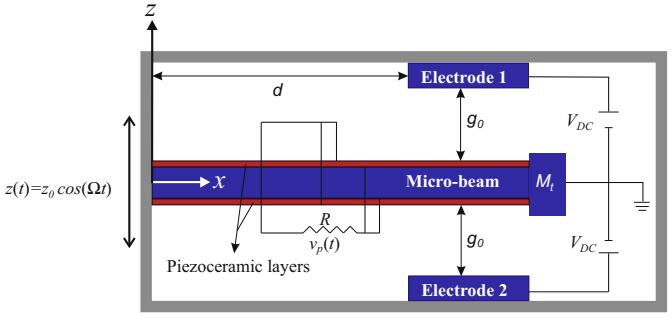

Fig. 1. Schematic of the proposed energy harvester.

$$(EI)_{eq}\frac{\partial^4 w(x,t)}{\partial x^4}+(\rho A)_{eq}\frac{\partial^2 w(x,t)}{\partial t^2}+c_a\frac{\partial w(x,t)}{\partial t}-\vartheta\, v(t)\left(\frac{d\delta(x)}{dx}-\frac{d\delta(x-L)}{dx}\right)$$
$$=\frac{\varepsilon_0 a\, H(x-d)}{2}\left(\frac{V_{DC}^2}{(g_0-w)^2}-\frac{V_{DC}^2}{(g_0+w)^2}\right)-\big((\rho A)_{eq}+M_t\delta(x-L)\big)\frac{\partial^2 z(t)}{\partial t^2} \tag{1}$$

where

$$(EI)_{eq}=\frac{2a}{3}\left(E\frac{h^3}{8}+E_0\left(\left(h_0+\frac{h}{2}\right)^3-\frac{h^3}{8}\right)\right),\quad (\rho A)_{eq}=a\big(\rho h+2\rho_0 h_0\big)$$

and subjected to the following boundary conditions:

$$w(0,t)=0,\quad \frac{\partial w(0,t)}{\partial x}=0$$
$$\frac{\partial}{\partial x}\left((EI)_{eq}\frac{\partial^2 w(L,t)}{\partial x^2}\right)=M_t\left(\frac{\partial^2 w(L,t)}{\partial t^2}\right)$$
$$(EI)_{eq}\frac{\partial^2 w(L,t)}{\partial x^2}=-I_{M_t}\frac{\partial^2}{\partial t^2}\left(\frac{\partial w(L,t)}{\partial x}\right) \tag{2}$$

In Eq. (1), $w(x,t)$ is the transverse deflection of the beam relative to its base at the position x and time t, c_a is the viscous air damping coefficient, ε_0 is the permittivity of free space, $H(x)$ is the Heaviside function, $\delta(x)$ is the Dirac delta function, V_{DC} is the applied DC voltage to microbeam, g_0 is the air gap between electrodes (the system is assumed to be symmetric), $z(t)$ is the base excitation function, $v(t)$ is the voltage across the electrodes of each piezoceramic layer and ϑ is the coupling term which is dependent on the type of connection between the piezoceramic layers (i.e. series or parallel connections). In series, the two piezoelectric layers are oppositely polarized and produce a larger voltage output; whereas in parallel, the two piezoelectric layers are polarized in the same direction, and a larger current output is achievable. For the series and parallel connection cases the piezoelectric coupling term can be respectively expressed as [30]

$$\vartheta_s=\frac{\bar{e}_{31}a}{2h_0}\left(\left(h_0+\frac{h}{2}\right)^2-\frac{h^2}{4}\right)$$
$$\vartheta_p=2\vartheta_s=\frac{\bar{e}_{31}a}{h_0}\left(\left(h_0+\frac{h}{2}\right)^2-\frac{h^2}{4}\right) \tag{3}$$

where subscripts s and p denote series and parallel connections of the piezoceramic layers respectively and $\bar{e}_{31}$ is the equivalent piezoelectric coefficient. By considering the parallel connection between these layers and $z_0\cos(\Omega t)$ as a base excitation, Eq. (1) can be written as

$$(EI)_{eq}\frac{\partial^4 w(x,t)}{\partial x^4}+(\rho A)_{eq}\frac{\partial^2 w(x,t)}{\partial t^2}+c_a\frac{\partial w(x,t)}{\partial t}$$
$$-\vartheta_p\, v_p(t)\left(\frac{d\delta(x)}{dx}-\frac{d\delta(x-L)}{dx}\right)=\frac{\varepsilon_0 a\, H(x-d)}{2}\left(\frac{V_{DC}^2}{(g_0-w)^2}-\frac{V_{DC}^2}{(g_0+w)^2}\right)$$
$$+z_0\Omega^2\big((\rho A)_{eq}+M_t\delta(x-L)\big)\cos(\Omega t) \tag{4}$$

and the electrical circuit equation (see Fig. 2) based on Kirchhoff's laws can be expressed as

$$C_p\frac{dv_p(t)}{dt}+\frac{v_p(t)}{2R}+i_p(t)=0 \tag{5}$$

where the internal capacitance (C_p) and the current source can be obtained as [30]

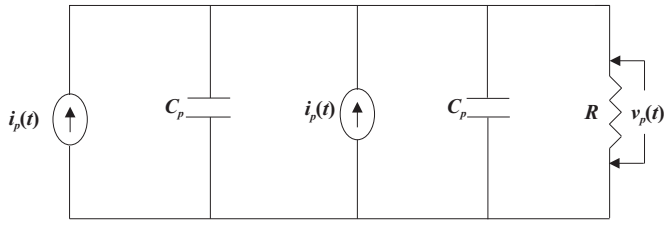

Fig. 2. Electrical circuit showing the parallel connection of the piezoceramic layers.

$$C_p=\frac{\bar{\varepsilon}_{33}^{s} aL}{h_0},\ i_p(t)=\frac{\bar{e}_{31} a}{2}(h_0+h)\int_0^L \frac{\partial^3 w(x,t)}{\partial x^2 \partial t}dx \tag{6}$$

and $\bar{\varepsilon}_{33}^{s}$ is the permittivity component at constant strain with the plane stress assumption for the beam.

It is obvious from Eq. (4) that the electrostatic force is an inherent source of nonlinearity. In order to investigate the nonlinearity, the total deflection of the microbeam can be considered as

$$w(x,t)=w_{st}(x)+\mathrm{w_d}(x,t) \tag{7}$$

By Substituting Eq. (7) into Eqs. (4) and (5) and using a Taylor series expansion about the equilibrium position (w_{st}=0) up to the ninth-order, the following equations are obtained

$$(EI)_{\mathrm{eq}}\frac{\partial^4 w_d}{\partial t^4}+(pA)_{\mathrm{eq}}\frac{\partial^2 w_d}{\partial t^2}+c_a\frac{\partial w_d}{\partial t}-\vartheta_p v_p(t)\left(\frac{d\delta(x)}{dx}-\frac{d\delta(x-L)}{dx}\right)$$
$$=\frac{\varepsilon_0 a V_{DC}^2 H(x-d)}{2}\left(\frac{4w_d}{g_0^3}+\frac{8w_d^3}{g_0^5}+\frac{12w_d^5}{g_0^7}+\frac{16w_d^7}{g_0^9}+\frac{20w_d^9}{g_0^{11}}+\dots\right)$$
$$+z_0\Omega^2\big((\rho A)_{eq}+M_t\delta(x-L)\big)\cos(\Omega t) \tag{8a}$$

$$C_p\frac{dv_p(t)}{dt}+\frac{v_p(t)}{2R}+\frac{\bar{e}_{31} a}{2}(h_0+h)\int_0^L \frac{\partial^3 \mathrm{w_d}}{\partial x^2\partial t}dx=0 \tag{8b}$$

2.1. Reduced-order model

In this subsection, the Galerkin decomposition method is used to eliminate the spatial dependence. To this end, the deflection of the microbeam can be represented as a series expansion in terms of the eigenfunctions of the microbeam, i.e.

$$\mathrm{w_d}(x,t)=\sum_{i=1}^{N} U_i(t)\varphi_i(x) \tag{9}$$

where $\varphi_i(x)$ is the ith linear undamped mode shape of the straight microbeam and $U_i(t)$ is the ith generalized coordinate. Eqs. (8a) and (8b) can be converted into a system of differential equations using this method. A single-mode approximation yields the following equations:

$$M\ddot{U}(t)+C\dot{U}(t)+\big(K_m+K_e\big)U(t)-\theta_p v_p(t)+K_{n1}U^3(t)+K_{n2}U^5(t)+K_{n3}U^7(t)+K_{n4}U^9(t)=F_b\cos(\Omega t) \tag{10a}$$

$$\dot{v}_p(t)+\lambda v_p(t)+\kappa\dot{U}(t)=0 \tag{10b}$$

where

$$M=(\rho A)_{eq}\int_0^L\varphi^2(x)dx,\ C=c_a\int_0^L\varphi^2(x)dx,\ K_m=(EI)_{eq}\int_0^L\varphi(x)\varphi^{IV}(x)dx,$$
$$K_e=-\frac{2\varepsilon_0 a V_{DC}^2\int_0^L\varphi^2(x)H(x-d)dx}{g_0^3},\ \theta_p=\vartheta_p\left(\frac{d\varphi(L)}{dx}-\frac{d\varphi(0)}{dx}\right),$$
$$K_{n1}=-\frac{4\varepsilon_0 a V_{DC}^2\int_0^L\varphi^4(x)H(x-d)dx}{g_0^5},\ K_{n2}=-\frac{6\varepsilon_0 a V_{DC}^2\int_0^L\varphi^6(x)H(x-d)dx}{g_0^7},$$
$$K_{n3}=-\frac{8\varepsilon_0 a V_{DC}^2\int_0^L\varphi^8(x)H(x-d)dx}{g_0^9},\ K_{n4}=-\frac{10\varepsilon_0 a V_{DC}^2\int_0^L\varphi^{10}(x)H(x-d)dx}{g_0^{11}},$$
$$F_b=z_0\Omega^2\left((\rho A)_{eq}\int_0^L\varphi(x)dx+M_t\int_0^L\varphi(x)\delta(x-L)dx\right),$$
$$\lambda=\frac{1}{2RC_p},\ \kappa=\frac{\bar{e}_{31} a(h_0+h)}{2C_p}\left(\frac{d\varphi(L)}{dx}\right) \tag{10c}$$

Eq. (10a) can be rewritten as:

$$\ddot{U}(t)+2\mu\omega_n\dot{U}(t)+\omega_n^2U(t)-\chi v_p(t)+\alpha U^3(t)+\beta U^5(t)+\gamma U^7(t)+\delta U^9(t)=F\cos(\Omega t) \tag{11a}$$

where

$$\mu=\frac{C}{2M\omega_n},\quad \omega_n=\sqrt{\frac{K_m+K_e}{M}},\quad \chi=\frac{\theta_p}{M},\quad \alpha=\frac{K_{n1}}{M},\quad \beta=\frac{K_{n2}}{M},$$
$$\gamma=\frac{K_{n3}}{M},\quad \delta=\frac{K_{n4}}{M},\quad F=\frac{F_b}{M} \tag{11b}$$

Eq. (10a) shows that the electrostatic forces create a negative stiffness which opposes the mechanical stiffness. Above a certain applied DC voltage, electrostatic MEMS devices can become unstable. This voltage is known as the pull-in voltage [31].

2.2. Harmonic balance analyses

To determine the analytical solution of Eqs. (11a) and (10b), the method of harmonic balance is used. By assuming a steady state periodic response, $U(t)$ and $v_p(t)$ can be written as:

$$U(t)=a_1(t)\sin(\Omega t)+b_1(t)\cos(\Omega t) \tag{12a}$$
$$v_p(t)=a_2(t)\sin(\Omega t)+b_2(t)\cos(\Omega t) \tag{12b}$$

with slowly varying coefficients such that

$$\dot{U}(t)=\left(\dot{b}_1+a_1\Omega\right)\cos(\Omega t)+\left(\dot{a}_1-b_1\Omega\right)\sin(\Omega t) \tag{13a}$$

$$\dot{v}_p(t)=\left(\dot{b}_2+a_2\Omega\right)\cos(\Omega t)+(\dot{a}_2-b_2\Omega)\sin(\Omega t) \tag{13b}$$

and

$$\ddot{U}(t)=\Omega\left(2\dot{a}_1-b_1\Omega\right)\cos(\Omega t)-\Omega\left(2\dot{b}_1+a_1\Omega\right)\sin(\Omega t) \tag{13c}$$

Substituting the above expressions into Eqs. (11a) and (10b), neglecting higher harmonics and balancing terms multiplied by $\sin(\Omega t)$ and $\cos(\Omega t)$, from the mechanical equation the following equations are obtained

$$2\mu\omega_n\dot{a}_1-2\Omega\dot{b}_1=Qa_1+\chi a_2+2\mu\omega_n b_1\Omega \tag{14a}$$

$$2\mu\omega_n\dot{b}_1+2\Omega\dot{a}_1=Qb_1+\chi b_2+F-2\mu\omega_n a_1\Omega \tag{14b}$$

where

$$r^2=a_1^2+b_1^2, \tag{15a}$$
$$Q=-\omega_n^2+\Omega^2-\frac{3}{4}\alpha r^2-\frac{5}{8}\beta r^4-\frac{35}{64}\gamma r^6-\frac{63}{128}\delta r^8 \tag{15b}$$

Applying the same approach to the electrical equation yields

$$\kappa\dot{a}_1+\dot{a}_2=b_2\Omega-\lambda a_2+\kappa b_1\Omega \tag{16a}$$
$$\kappa\dot{b}_1+\dot{b}_2=-a_2\Omega-\lambda b_2-\kappa a_1\Omega \tag{16b}$$

In steady state, all time derivatives vanish so that we can re-write the mechanical amplitude equations as

$$0=Qa_1+\chi a_2+2\mu\omega_n b_1\Omega \tag{17a}$$
$$0=Qb_1+\chi b_2+F-2\mu\omega_n a_1\Omega \tag{17b}$$

and the electrical amplitude equations as

$$0=b_2\Omega-\lambda a_2+\kappa b_1\Omega \tag{18a}$$
$$0=a_2\Omega+\lambda b_2+\kappa a_1\Omega \tag{18b}$$

The electrical coefficients a_2 and b_2 can be obtained from Eqs. (18a) and (18b) as

$$a_2=\frac{\kappa\Omega}{\Omega^2+\lambda^2}(\lambda b_1-a_1\Omega) \tag{19a}$$
$$b_2=-\frac{\kappa\Omega}{\Omega^2+\lambda^2}(\lambda a_1+b_1\Omega) \tag{19b}$$

Substituting the steady-state solutions for a_2 and b_2 into the steady-state equations for a_1 and b_1 yields

$$0=\Lambda_a a_1+\Lambda_b b_1 \tag{20a}$$

$$F=\Lambda_b a_1-\Lambda_a b_1 \tag{20b}$$

where

$$\Lambda_a=Q-\frac{\kappa\chi\Omega^2}{\Omega^2+\lambda^2} \tag{21a}$$

$$\Lambda_b=2\mu\omega_n\Omega+\frac{\kappa\chi\lambda\Omega}{\Omega^2+\lambda^2} \tag{21b}$$

squaring and adding Eqs. (20a) and (20b) gives an eighteenth order nonlinear algebraic equation in r as

$$F^2=r^2(\Lambda_a^2+\Lambda_b^2) \tag{22}$$

and the frequency response can be determined by numerically finding the positive real roots of Eq. (22). Similarly, by squaring and adding Eqs. (19a) and (19b), the response voltage amplitude can be written in terms of the mechanical amplitude as

$$S=r\sqrt{\Gamma_a^2+\Gamma_b^2} \tag{23}$$

where

$$\Gamma_a=\frac{\kappa\lambda\Omega}{\Omega^2+\lambda^2} \tag{24a}$$

$$\Gamma_b=\frac{\kappa\Omega^2}{\Omega^2+\lambda^2} \tag{24b}$$

and r is an implicit function of the forcing amplitude, damping, electromechanical coupling, and electrical dissipation as derived from the roots of Eq. (22). The peak power through the resistance can then be written as

$$P_0=\frac{S^2}{R} \tag{25}$$

and the average power is

$$\bar{P}_0=\frac{S^2}{2R} \tag{26}$$

2.3. Stability analysis

In this subsection a stability analysis is provided because only a few solutions of the eighteen total roots for r in Eq. (22) can be realized in practice. In order to ascertain the stability of the solutions, it is first necessary to rewrite Eqs.(14a),(14b), (16a) and (16b) in the matrix form

$$\mathbf{A}\dot{\mathbf{x}}=\mathbf{D}(\mathbf{x}) \tag{27a}$$

where

$$\mathbf{A}=\begin{bmatrix} 2\mu\omega_n & -2\Omega & 0 & 0 \\ 2\Omega & 2\mu\omega_n & 0 & 0 \\ \kappa & 0 & 1 & 0 \\ 0 & \kappa & 0 & 1 \end{bmatrix},\ \mathbf{D}(\mathbf{x})=\begin{bmatrix} Qa_1+\chi a_2+2\mu\omega_n b_1\Omega \\ Qb_1+\chi b_2+F-2\mu\omega_n a_1\Omega \\ b_2\Omega-\lambda a_2+\kappa b_1\Omega \\ -a_2\Omega-\lambda b_2-\kappa a_1\Omega \end{bmatrix} \tag{27b}$$

with the vector $\mathbf{x}=[a_1 b_1 a_2 b_2]^{\mathrm{T}}$. One may write Eq. (27a) as

$$\dot{\mathbf{x}}=\mathbf{G}(\mathbf{x}) \tag{28a}$$

where $\mathbf{G}(\mathbf{x})=\mathbf{A}^{-1}\mathbf{D}(\mathbf{x})$. The stability can be investigated by constructing the Jacobian matrix of $\mathbf{G}(\mathbf{x})$ and calculating its value at the steady state values for $\mathbf{x}$, which are indicated as $\mathbf{x}_{ss}$

$$\mathbf{J}=\frac{\partial\mathbf{G}}{\partial\mathbf{x}}\Big|_{\mathbf{x}=\mathbf{x}_{ss}} \tag{29}$$

The values for $\mathbf{x}_{ss}$ can be found through solutions of Eqs. (17a)–(18b). By evaluating the eigenvalues of the Jacobian matrix, the stability of the steady state solutions is determined. If all of the eigenvalues associated with the steady state solution have negative real parts then the solution is asymptotically stable. Otherwise, if one eigenvalue has a positive real part then, the solution is unstable.

3. Numerical results and discussion

To demonstrate the analysis presented in Sections 2.1 and 2.2, shape functions, which satisfy the boundary conditions of the clamped-free microbeam (with tip mass M_t), are considered of the form [30]

$$\varphi_i(x)=A_r\left[\cos\lambda_i\frac{x}{L}-\cosh\lambda_i\frac{x}{L}+\varsigma_r\left(\sin\lambda_i\frac{x}{L}-\sinh\lambda_i\frac{x}{L}\right)\right] \tag{30a}$$

where

$$\varsigma_r=\frac{\sin\lambda_i-\sinh\lambda_i+\lambda_i\frac{M_t}{(\rho A)_{eq}L}(\cos\lambda_i-\cosh\lambda_i)}{\cos\lambda_i+\cosh\lambda_i-\lambda_i\frac{M_t}{(\rho A)_{eq}L}(\sin\lambda_i-\sinh\lambda_i)} \tag{30b}$$

A_r is the modal amplitude constant and the eigenvalues of the system (λ_i for mode i) are obtained from

$$1+\cos\lambda_i\cosh\lambda_i+\lambda_i\frac{M_t}{(\rho A)_{eq}L}(\cos\lambda_i\sinh\lambda_i-\sin\lambda_i\cosh\lambda_i)-\frac{\lambda_i^3 I_t}{(\rho A)_{eq}L^3}(\cosh\lambda_i\sin\lambda_i+\sinh\lambda_i\cos\lambda_i)+\frac{\lambda_i^4 M_t I_t}{(\rho A)_{eq}L^3}(1-\cos\lambda_i\cosh\lambda_i)=0 \tag{31}$$

3.1. Parametric study

In order to investigate the effect of different parameters in the design of a tunable harvester, a clamped-free microbeam is considered with the characteristics given in Table 1.

The dynamic behavior of the system is affected by the nonlinearity of the electrostatic force and increasing the applied DC voltage or/and decreasing the initial gap can magnify this nonlinearity. Based on the Taylor expansion of this force at a constant initial gap, by increasing the applied DC voltages to the electrostatic electrodes, the electrical stiffness of the structure is increased and leads to the decrease of the equivalent stiffness of the structure (see Eq. (10c)). Consequently, at the critical value of the applied DC voltage called the pull-in voltage, the system has a static instability by undergoing a pitchfork bifurcation. On the other hand, decreasing the equivalent stiffness of the structure decreases the resonance frequency of the open circuit system [29]. In order to study the dynamic analysis of the harvester using the harmonic balance method (HBM), the electrostatic force is approximated by a Taylor series expansion. Fig. 3 illustrates that acceptable convergence can be obtained by including the terms up to ninth-order.

The presented results based on the ninth order nonlinearity are verified by numerical results. Fig. 4 shows a good agreement between the results obtained by harmonic balance and those achieved by time integration. In the numerical method, the exact form of the electrostatic force is considered.

According to the dynamic analysis of the system the peak output power can be obtained from Eq. (25). Adjusting the resonance frequency of the system to match the frequency of the base excitation will increase the harvested power. Also, choosing the appropriate resistance can increase the harvested power. As illustrated in Fig. 5a, the optimal resistance depends on the frequency of base excitation and Fig. 5b shows that the optimal resistance reduces as the frequency of the base

Table 1
Geometrical and material properties of the microbeam and piezoelectric layers.

Design variable	Value
Length (L)	3000 μm
Width (a)	1000 μm
Thickness (h)	4 μm
Thickness (h_0)	2 μm
Young's modulus (E)	169.6 GPa
Young's modulus (E_0)	65 GPa
Viscous air damping coefficient (c_a)	0.0002 N s/m
Poisson's ratio (υ)	0.06
Density of Si beam (ρ)	2330 kg/m^3
Density of PZT (ρ_0)	7800 kg/m^3
Equivalent piezoelectric coefficient ($\bar{e}_{31}$)	-11.18 Cm^{-2}
Permittivity component ($\bar{\varepsilon}^s_{33}$)	13.48 nF/m
Tip mass (M_t)	9.724×10^{-8} kg
Length of the tip mass (L_m)	20 μm
Thickness of the tip mass (h_m)	10 μm

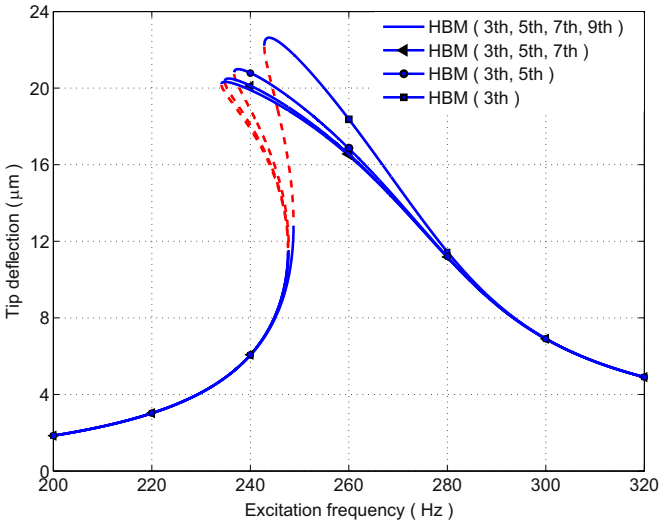

Fig. 3. Displacement frequency response curve for different orders of nonlinearity (g_0=30 μm, V_{DC}=8 V, R = 100 kΩ, L_e=0. 5 L, z_0=0.3 μm).

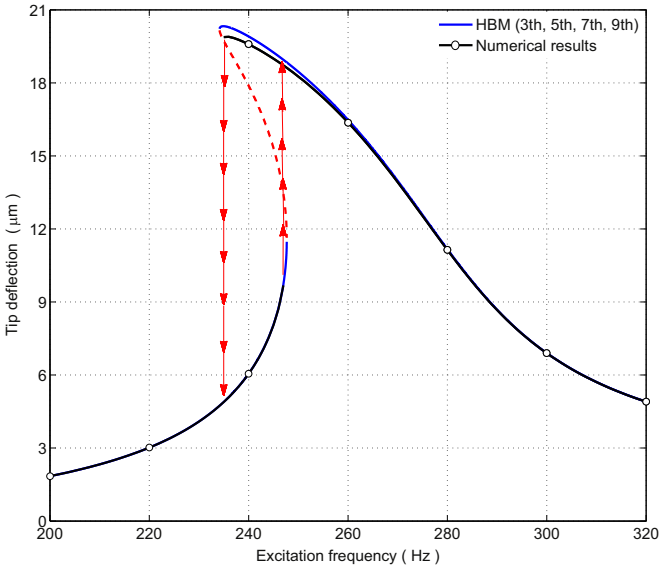

Fig. 4. Displacement frequency response curve (g_0=30 μm, V_{DC}=8 V, R = 100 kΩ, L_e=0. 5 L, z_0=0.3 μm).

excitation increases.

The dynamic behavior of the system can be affected by the applied DC voltage, the length of the electrode, the initial gap and the resistance. Therefore, these parameters can significantly affect the dynamic behavior of the system. Increasing the length of the electrodes or/and decreasing initial gap at constant voltage increases softening effect. However, it will decrease the harvested power. Fig. 6 investigates the effect of electrode length and resistance on the dynamics of the system at constant applied DC voltage.

As shown in Fig. 6a, the length of the electrode is a key parameter in changing the resonance frequency of the system and also the nonlinearity of the system is affected by this parameter. Moreover changing the value of the resistance changes the nonlinearity of the system (see Fig. 6b). Therefore, by considering constant values for initial gap and electrodes length, the resonance frequency of the harvester can be controlled by the applied DC voltage and resistance to maximize the harvested power.

Increasing the range of operation frequency of the harvester based on the increasing applied DC voltage and the length of the electrode is limited due to the pull-in instability. However increasing the electrostatic force decreases the vibration of the microbeam and leads to a decrease in the output power. Therefore, the system needs to be optimized for maximum harvested power. On the other hand, due to the softening nonlinearity there are three solutions for the beam response within the frequency range closed to resonance and in order to harvest maximum power the beam response should always occur at the higher of the two solutions and close to resonance (but not too close to risk jumping down to the low amplitude

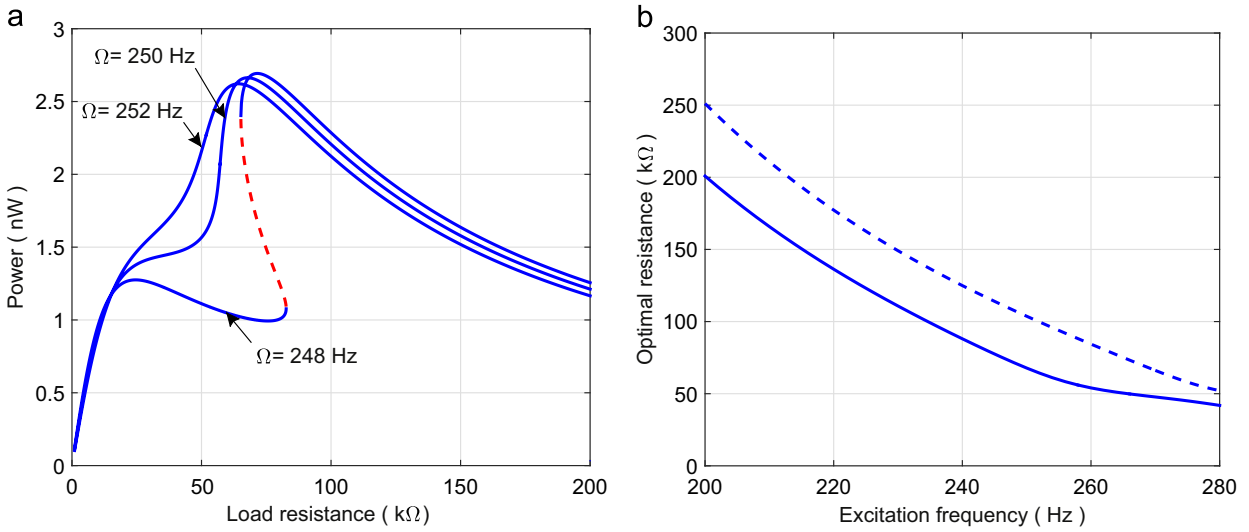

Fig. 5. (a) Variation of the piezoelectric peak power with load resistance for different frequencies of base excitation for V_{DC}=8 V (b) Variation of the optimal resistance for different frequencies of base excitation (g_0=30 μm, V_{DC}=8 V, L_e=0. 5 L, z_0=0.3 μm).

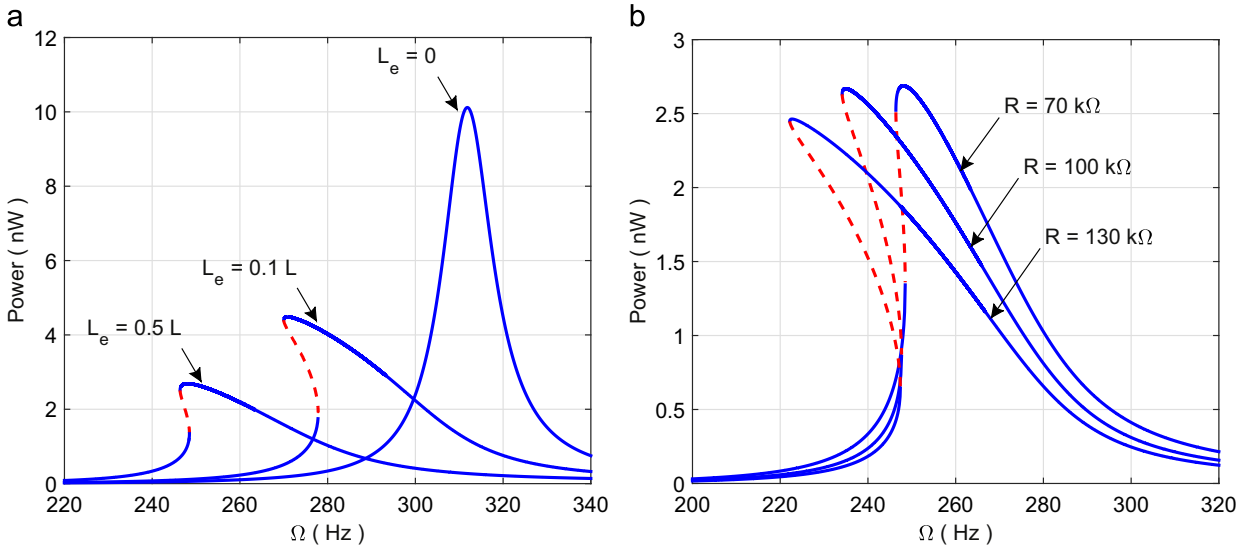

Fig. 6. Variation of the piezoelectric peak power with frequency of base excitation (g_0=30 μm, V_{DC}=8 V, z_0=0.3 μm). (a) $R = 70$ kΩ, (b) $L_e = 0.5\ L$.

solution). However the response at the high amplitude solution mostly depends on the initial conditions and hence it cannot be guaranteed. The control system using the applied DC voltage can be used to ensure the harvester always responds in the higher amplitude solution. For a given excitation frequency if the harvester response happens to be in the lower amplitude solution the DC voltage is increased until a region is reached where the harvester only has a single solution. The DC voltage is then slowly reduced and the harvester follows high amplitude solution until the resonance is obtained.

Fig. 7a shows that by varying the applied DC voltage to the electrodes, a frequency range between 312.2 Hz and 163.4 Hz is accessible. However the amount of variation in the voltages that requires covering the given range of operation frequency will be dependent upon the length of the electrodes, as shown in Fig. 7b.

In some cases, it is possible to have a vibration source with constant frequency and variable amplitude of base excitation. Fig. 8 investigates the variation of the output power when the excitation amplitude is changed at constant frequency. This figure shows that by increasing the amplitude of the base excitation the harvested power increases. However depending on the frequency of the vibration source, jumping is observed in some ranges of excitation amplitudes.

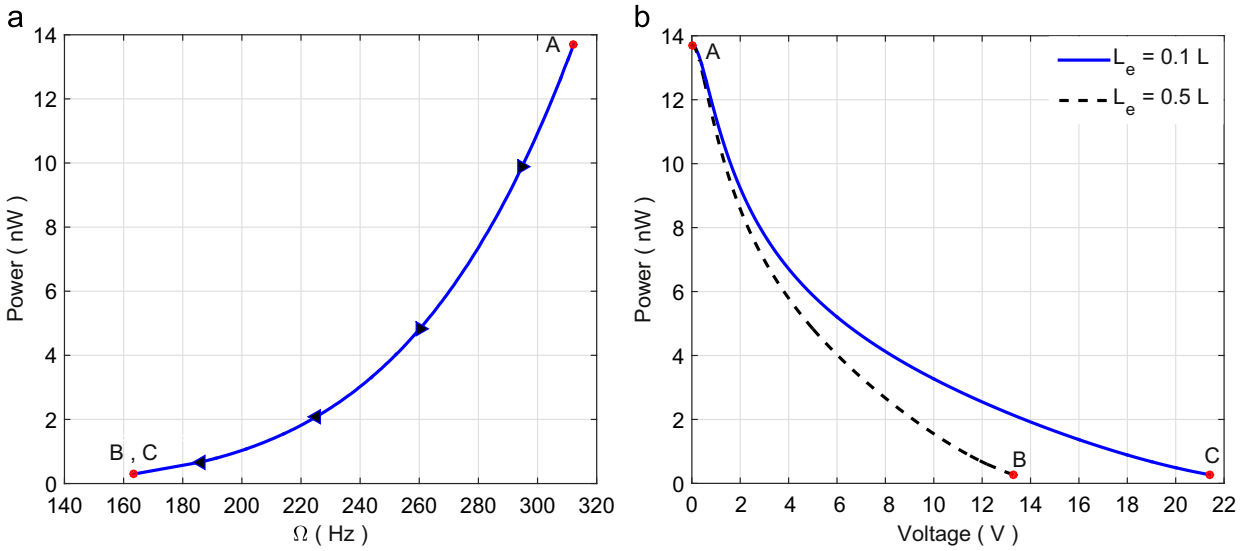

Fig. 7. (a) Frequency range of the harvester based on increasing DC voltage and (b) voltage range for different lengths of the electrodes to cover the frequency range (g_0=30 μm, R = 100 kΩ, z_0=0.3 μm).

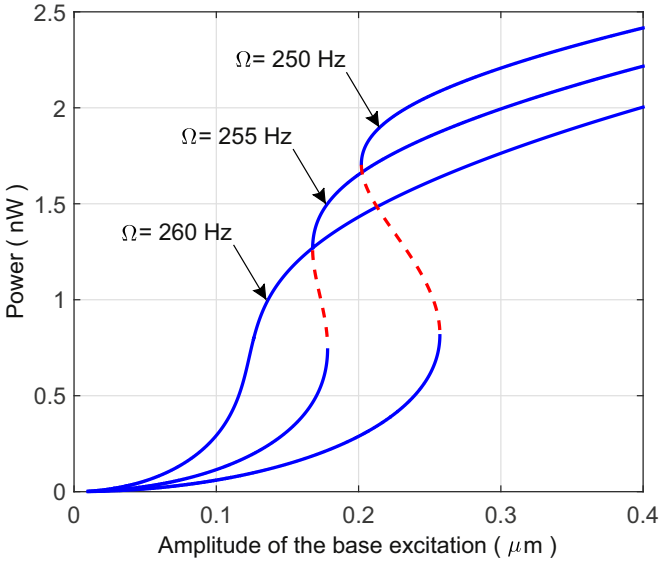

Fig. 8. Variation of the piezoelectric peak power with the frequency of base excitation (g_0=30 μm, V_{DC}=8 V, R = 100 kΩ, L_e=0. 5 L, z_0=0.3 μm).

3.2. Sustainability of the proposed harvester

In the proposed model the voltage source has been used to change the resonance frequency of the harvester. However this source can be charged by the harvested power from the electrostatic side. In general, electrostatic harvesters have passive structures which need an energy cycle to convert the mechanical energy into electrical energy [32,33]. Among different cycles proposed by researchers, there are two common cycles which use charge or voltage constraint concepts in the conversion cycle [34]. Fig. 1 shows that the proposed model consists of two variable capacitors which are connected to the same DC voltage. The variable capacitors are charged by V_{DC} and their capacitances can be expressed as

$$C_{v1}(t) = \frac{\varepsilon_0 A_e}{(g_0 + w_{av}(t))}, \quad C_{v2}(t) = \frac{\varepsilon_0 A_e}{(g_0 - w_{av}(t))} \tag{32}$$

where A_e is the overlapping area between the fixed and moveable electrodes and w_{av} is the average value of w in this area. The total amount of energy stored in the capacitors is

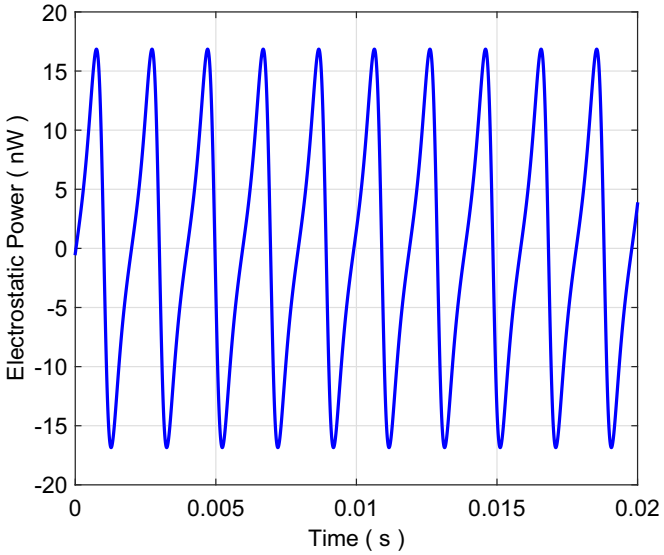

Fig. 9. Variation of the instantaneous electrostatic power with time (g_0=30 μm, V_{DC}=8 V, R = 100 kΩ, L_e=0. 1 L, z_0=0.3 μm, Ω=253 Hz).

Table 2
Geometrical properties of the microbeam and piezoelectric layer

Design variable	Value
Length (L)	4600 μm
Width (a)	2000 μm
Thickness (h)	3.005 μm
Thickness (h_0)	2 μm
Tip mass (M_t)	2.8108e − 07

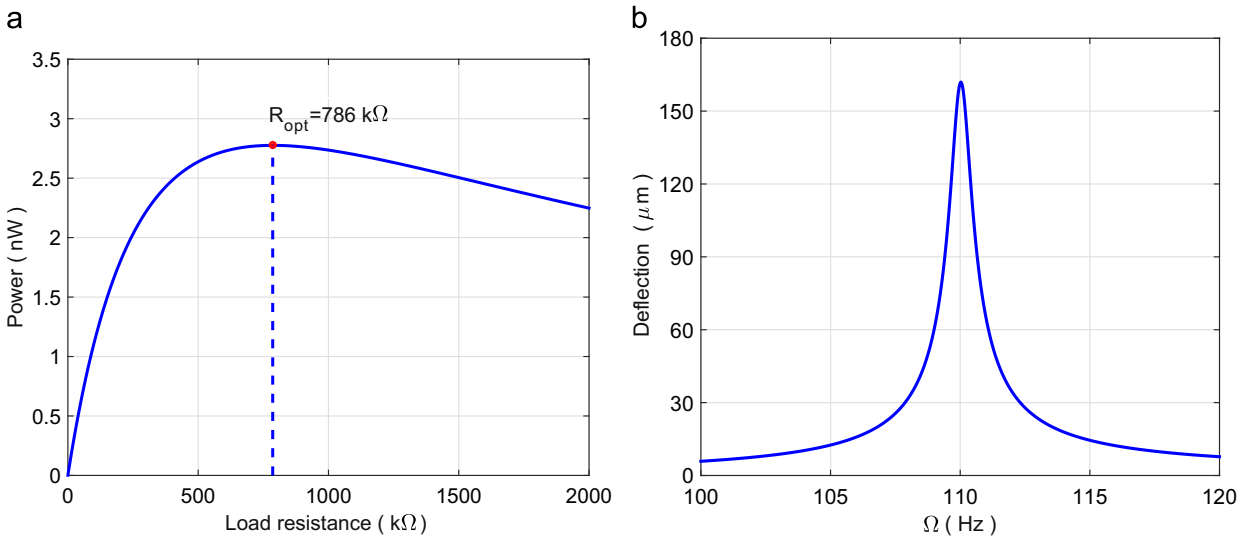

Fig. 10. (a) Variation of the piezoelectric peak power with load resistance for a linear harvester, and (b) displacement frequency response curve by considering optimal resistance (R = 786 kΩ).

$$U_t(\mathrm{t}) = \frac{1}{2}\left(C_{v1}(\mathrm{t}) + C_{v2}(\mathrm{t})\right)V_{DC}^2 \tag{33}$$

and consequently the generated instantaneous power can be presented by

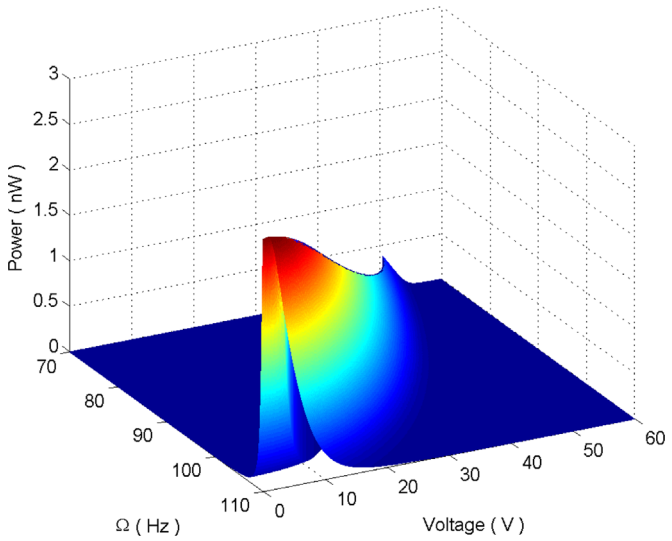

Fig. 11. Variation of the piezoelectric peak power with DC voltage (g_0=165 μm, L_e=0. 5 L, z_0=0.25 μm).

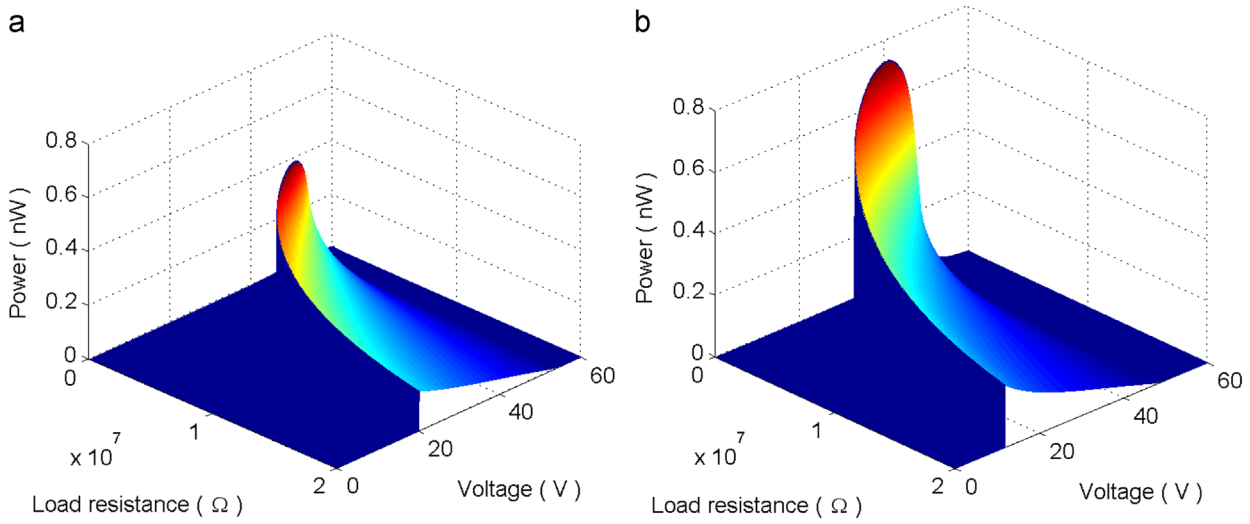

Fig. 12. Variation of the piezoelectric peak power by changing load resistance and voltage at 70 and 80 Hz (g_0=165 μm, L_e=0. 5 L, z_0=0.25 μm).

$$P_t(t) = \frac{dU_t}{dt} = \frac{\varepsilon_0 A_e V_{DC}^2}{2}\left(\frac{1}{(g_0 - w_{av}(t))^2} - \frac{1}{(g_0 + w_{av}(t))^2}\right)\frac{dw_{av}}{dt} \tag{34}$$

As illustrated in Fig. 9 the instantaneous power obtained from the capacitors varies between positive and negative values during each cycle. Therefore the voltage source is self-chargeable.

3.3. Design strategy

The design of the tuneable harvester should be preceded by an analyses of the source of vibration. There are two main design considerations. The first one is related to the maximum value of the excitation frequency (Ω_{max}) which is important in choosing the dimensions of the microbeam to match the resonance frequency of the harvester with Ω_{max}. The pull-in instability and the clearance between the electrodes are the second design factor. In addition, because of the strong coupling between the mechanical and electrical equations, the resistance can significantly change the mechanical behavior of the harvester. Therefore, this resistance is a key parameter in analyzing the vibration amplitude of the harvester. As an example, a source of vibration with a frequency range of 70–110 Hz and an amplitude of 0.25 μm is considered. According to the design considerations, the first step will be to choose the geometrical properties of the harvester to match maximum value of the excitation frequency (110 Hz). Like any other design problem, there is no unique solution. Table 2 gives one possibility. In order to choose the geometrical parameters, care has been taken to select reasonable dimensions. The dimensions that

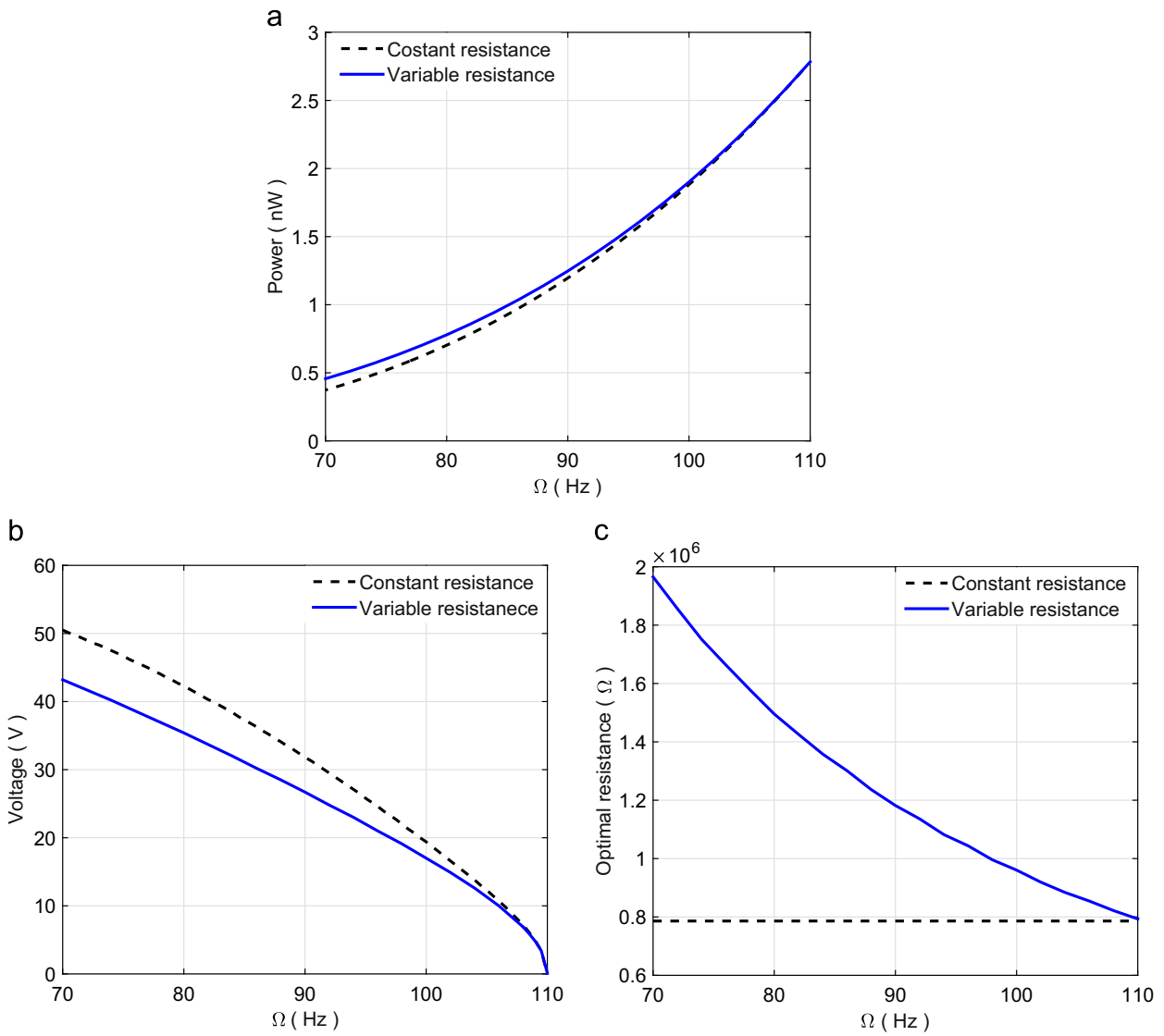

Fig. 13. (a) Frequency range of the harvester based on increasing DC voltage (b) voltage range for covering the frequency range and (c) optimal resistance at each frequency (g_0=165 μm, z_0=0.25 μm).

are used here are similar to those used in recent experimental and theoretical research papers [35,36].

The second step in designing the harvester is to find the optimal value of the resistance when the harvester works at Ω_{max}. As shown in Fig. 10a, without any electrostatic force the optimal resistance is 786 kΩ. In the third step, by analyzing the vibration response of the harvester the minimum initial gaps between electrodes can be determined to avoid any contact between the microbeam and the electrodes. Based on this analysis, the initial gap between the electrodes is 165 μm (see Fig. 10b).

In order to change the resonance frequency of the harvester, there are two possibilities, using only the variable voltage source or by simultaneously varying the load resistance and the voltages source. In the first case, the harvester is designed based on a constant load resistance. As shown in Fig. 11, by considering the optimal value of the resistance at Ω_{max} as a constant load resistance, the frequency range can be covered by changing the applied DC voltage from zero up to 50.5 V. The pull-in voltage of the microbeam is greater than 50.5 V and the clearance between the electrodes is considered at the second step.

According to Fig. 5b, by decreasing the frequency of excitation the optimal value of the resistance will be increased. On the other hand, based on Fig. 6b increasing the value of load resistance increases the softening effect and this can be considered as a second frequency adjusting parameter. Therefore, in the second case, the harvester is designed based on finding the optimal load resistance at each frequency of excitation. Fig. 12 shows the harvested power by considering the variable load resistance and voltage source at 70 and 80 Hz. Choosing suitable values for the load resistance and the applied DC voltage can increase the harvested power. At 70 Hz, the harvested power can be maximized by applying 43.6 V and using 1.9 MΩ load resistance. However in order to increase the harvested power at 80 Hz, the tuning parameters can be considered as V_{DC}=35. 3 V and R=1.5 MΩ.

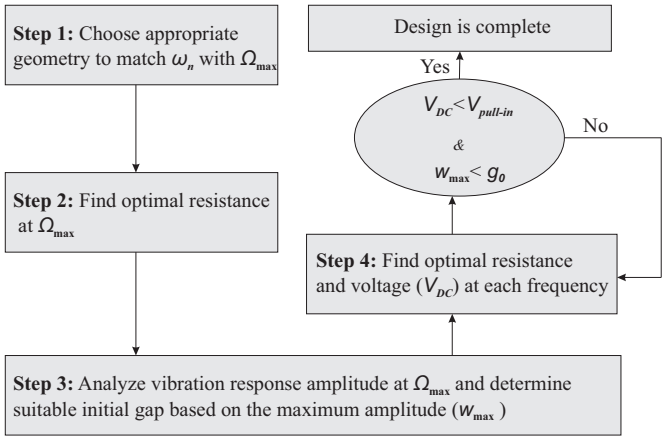

Fig. 14. Design flow chart.

By comparing the results of the two cases, the harvested power can be increased by using variable resistance and the difference is more obvious when the operational frequency range of the harvester is increased (see Fig. 13a). In addition, as shown in Fig. 14b, using the variable resistance decreases the range of voltage source required to cover the given frequency range. In general, the design process can be divided into four steps which are shown in Fig. 14.

4. Conclusions

In this paper, the design of a MEMS piezoelectric harvester, capable of adjusting its resonance frequency to the excitation frequency, is studied. The steady state solution is obtained by using the harmonic balance method and the results were verified numerically. It was observed that the analytical solution can lead to significant savings in computational time, particularly when there is a need for multiple runs, for example performing parametric studies for design purposes. Although the analytical solution requires an approximation to the electrostatic force by using a truncated Taylor's series, a convergence study can determine the number of terms that have to be retained in order to maintain sufficient accuracy. The results showed that the operating frequency bandwidth of the harvester can be increased by using a variable DC voltage source. In addition, due to the strong coupling between electrical and mechanical equations, the results showed that the load resistance can be considered as a second adjusting frequency parameter. A MEMS piezoelectric harvester was designed for a vibration source with a frequency range of 70–110 Hz and 0.25 μm amplitude of base excitation. The disadvantage of the proposed system is the effect of the softening nonlinearity of the electrostatic part of the harvester which results in a lower level of harvested energy. Future work includes devising a mechanism that has a hardening effect on the system and hence the frequency can be adjusted on both sides of its linear natural frequency.

Acknowledgments

Hadi Madinei acknowledges the financial support from the Swansea University, United Kingdom through the award of the Zienkiewicz scholarship.

References

[1] P.L. Green, E. Papatheou, N.D. Sims, Energy harvesting from human motion and bridge vibrations: an evaluation of current nonlinear energy harvesting solutions, J. Intell. Mater. Syst. Struct. 24 (12) (2013) 1494–1505.
[2] P.L. Green, K. Worden, N.D. Sims, On the identification and modelling of friction in a randomly excited energy harvester, J. Sound Vib. 332 (19) (2013) 4696–4708.
[3] X. Wang, X. Liang, G. Shu, S. Watkins, Coupling analysis of linear vibration energy harvesting systems, Mech. Syst. Signal Process. 70–71 (2016) 428–444.
[4] G. Gatti, M.J. Brennan, M.G. Tehrani, D.J. Thompson, Harvesting energy from the vibration of a passing train using a single-degree-of-freedom oscillator, Mech. Syst. Signal Process. 66–67 (2016) 785–792.
[5] A.S. De Paula, D.J. Inman, Marcelo A. Savi, Energy harvesting in a nonlinear piezomagnetoelastic beam subjected to random excitation, Mech. Syst. Signal Process. 54–55 (2015) 405–416.
[6] M. Borowiec, G. Litak, M.I. Friswell, S. Adhikari, Energy harvesting in a nonlinear cantilever piezoelastic beam system excited by random vertical vibrations, Int. J. Struct. Stab. Dyn. 14 (8) (2014) 1440018.
[7] K. Vijayan, M.I. Friswell, H.H. Khodaparast, S. Adhikari, Non-linear energy harvesting from coupled impacting beams, Int. J. Mech. Sci. 96–97 (2015) 101–109.
[8] Ö. Zorlu, E.T. Topal, H. Külah, A vibration-based electromagnetic energy harvester using mechanical frequency up-conversion method, IEEE Sens. J. 11

(2) (2011) 481–488.
[9] T. Galchev, E.E. Aktakka, K. Najafi, A piezoelectric parametric frequency increased generator for harvesting low-frequency vibrations, IEEE J. Microelectromech. Syst. 21 (2012) 1311–1320.
[10] M.F. Lumentut, I.M. Howard, Analytical and experimental comparisons of electromechanical vibration response of a piezoelectric bimorph beam for power harvesting, Mech. Syst. Signal Process. 36 (1) (2013) 66–86.
[11] X. Wang, X. Liang, Z. Hao, H. Du, N. Zhang, M. Qian, Comparison of electromagnetic and piezoelectric vibration energy harvesters with different interface circuits, Mech. Syst. Signal Process. 72–73 (2016) 906–924.
[12] D. Hoffmann, B. Folkmer, Y. Manoli, Fabrication, characterization and modelling of electrostatic micro-generators, J. Micromech. Microeng. 19 (2009) 094001.
[13] M. Defosseux, M. Allain, E. Defay, S. Basrour, Highly efficient piezoelectric micro harvester for low level of acceleration fabricated with a CMOS compatible process, Sens. Actuator A Phys. 188 (2012) 489–494.
[14] T. Galchev, E.E. Aktakka, K. Najafi, A piezoelectric parametric frequency increased generator for harvesting low-frequency vibrations, IEEE/ASME J. Microelectromech. Syst. 21 (6) (2012) 1311–1320.
[15] R. Andosca, T. McDonald, V. Genova, S. Rosenberg, J. Keating, C. Benedixen, J. Wu, Experimental and theoretical studies on MEMS piezoelectric vibrational energy harvesters with mass loading, Sens. Actuator A Phys. 178 (2012) 76–87.
[16] Y.B. Jeon, R. Sood, J.H. Jeong, S.G. Kim, MEMS power generator with transverse mode thin film PZT, Sens. Actuators A: Phys. 122 (1) (2005) 16–22.
[17] W.J. Choi, Y. Jeon, J.H. Jeong, R. Sood, S.G. Kim, Energy harvesting MEMS device based on thin film piezoelectric cantilevers, J. Electroceram. 17 (2006) 543–548.
[18] M. Renaud, K. Karakaya, T. Sterken, P. Fiorini, C. Van Hoof, R. Puers, Fabrication, modelling and characterization of MEMS piezoelectric vibration harvester, Sens. Actuators A: Phys. 145–146 (2008) 380–386.
[19] D. Shen, J. Park, J. Ajitsaria, S. Choe, H. Wikle, D. Kim, The design, fabrication and evaluation of a MEMS PZT cantilever with an integrated Si proof mass for vibration energy harvesting, J. Micromech. Microeng. 18 (2008) 055017.
[20] J.M. Youngsman, T. Luedeman, D.J. Morris, M.J. Anderson, D.F. Bahr, A model for an extensional mode resonator used as a frequency-adjustable vibration energy harvester, J. Sound Vib. 329 (3) (2010) 277–288.
[21] H. Xue, Y. Hu, Q.-M. Wang, Broadband piezoelectric energy harvesting devices using multiple bimorphs with different operating frequencies, IEEE Trans. Ultrason. Ferroelectr. Freq. Control 55 (9) (2008) 2104–2108.
[22] A. Erturk, J. Hoffmann, D.J. Inman, A piezomagnetoelastic structure for broadband vibration energy harvesting, Appl. Phys. Lett. 94 (254102) (2009) 1–3.
[23] M. Ghandchi Tehrani, S.J. Elliott, Extending the dynamic range of an energy harvester using nonlinear damping, J. Sound Vib. 333 (3) (2014) 623–629.
[24] B.P. Mann, N.D. Sims, Energy harvesting from the nonlinear oscillations of magnetic levitation, J. Sound Vib. 319 (2009) 515–530.
[25] M. Marzencki, M. Defosseux, S. Basrour, MEMS vibration energy harvesting devices with passive resonance frequency adaptation capability, J. Microelectromech. Syst. 18 (6) (2009) 1444–1453.
[26] D. Zhu, S. Roberts, M.J. Tudor, S.P. Beeby, Design and experimental characterization of a tunable vibration-based electromagnetic micro-generator, Sens. Actuators A 158 (2010) 284–293.
[27] V.R. Challa, M.G. Prasad, F.T. Fisher, Towards an autonomous self-tuning vibration energy harvesting device for wireless sensor network applications, Smart Mater. Struct. 20 (2) (2011) 025004.
[28] L.M. Miller, P. Pillatsch, E. Halvorsen, P.K. Wright, E.M. Yeatman, A.S. Holmes, Experimental passive self-tuning behavior of a beam resonator with sliding proof mass, J. Sound Vib. 332 (2013) 7142.
[29] H. Madinei, H.H. Khodaparast, S. Adhikari, M.I. Friswell, M. Fazeli, Adaptive tuned piezoelectric MEMS vibration energy harvester using an electrostatic device, Eur. Phys. J. Spec. Top. 224 (2015) 2703–2717.
[30] A. Erturk, D.J. Inman, Piezoelectric Energy Harvesting, John Wiley & Sons, Chichester, UK, 2011.
[31] H. Madinei, G. Rezazadeh, S. Azizi, Stability and bifurcation analysis of an asymmetrically electrostatically actuated microbeam, J. Comput. Nonlinear Dyn. 10 (2) (2015) 021002.
[32] E. Torres, G. Rincon-Mora, Electrostatic energy harvester and Li-ion charger circuit for micro-scale applications, in: Proceedings of the 49th IEEE Circuits and Systems on MWSCAS '06, 2006, pp. 65–69.
[33] P.D. Mitcheson, P. Miao, B.H. Stark, E.M. Yeatman, A.S. Holmes, T.C. Green, MEMS electrostatic micropower generator for low frequency operation, Sens. Actuators A: Phys. 115 (2–3) (2004) 523–529.
[34] S. Meninger, J.O. Mur-Miranda, R. Amirtharajah, A. Chandrakasan, J.H. Lang, Vibration-to-electric energy conversion, IEEE Trans. Very Large Scale Integr. ((VLSI)) Syst. 9 (1) (2001) 64–76.
[35] N. Jaber, A. Ramini, A.A.A. Carreno, M.I. Younis, Higher order modes excitation of electrostatically actuated clamped–clamped microbeams: experimental and analytical investigation, J. Micromech. Microeng. 26 (2) (2016) 025008.
[36] Hua-Bin Fang, Jing-Quan Liu, Zheng-Yi Xu, Lu Dong, Li Wang, Di Chen, Bing-Chu Cai, Yue Liu, Fabrication and performance of MEMS-based piezoelectric power generator for vibration energy harvesting, Microelectron. J. 37 (11) (2006) 1280–1284.